952431

A New High Pressure Droplet Vaporization Model for Diesel Engine Modeling

E. W. Curtis, A. Uludogan, and R. D. Reitz
Department of Mechanical Engineering
University of Wisconsin - Madison
Madison, WI 53706

ABSTRACT

A droplet vaporization model has been developed for use in high pressure spray modeling. The model is a modification of the common Spalding vaporization model that accounts for the effects of high pressure on phase equilibrium, transport properties, and surface tension. The new model allows for a nonuniform temperature within the liquid by using a simple 2-zone model for the droplet. The effects of the different modifications are tested both for the case of a single vaporizing droplet in a quiescent environment as well as for a high pressure spray using the KIVA II code. Comparisons with vaporizing spray experiments show somewhat improved spray penetration predictions. Also, the effect of the vaporization model on diesel combustion predictions was studied by applying the models to simulate the combustion process in a heavy duty diesel engine. In this case the standard and High Pressure vaporization models were found to give similar heat release and emissions results. However, the results show that a more realistic representation of the vaporization process is achieved with the new model. In particular, less unburned fuel is predicted to remain in the combustion chamber late in the power stroke.

INTRODUCTION

In many combustion systems a spray of small fuel droplets is injected into an oxidizing gas stream. In diesel engines the formation of droplets, droplet breakup and then vaporization are important processes that determine the rate of combustion and the delay between the start of injection and the start of combustion (ignition delay) [1]*. The distribution and concentration of fuel vapor in the combustion chamber directly affect the combustion efficiency, performance and emissions of the combustion system [2]. If the vaporization and combustion characteristics of the fuel spray were known in detail, the design of fuel injection systems and combustion chambers could be optimized efficiently without the need for extensive experimental trial and error. Thus, there is an interest in developing models of the spray combustion process.

In modern spray combustion computer models such as the KIVA II code [3] the droplet vaporization model, spray breakup model and combustion model are all interdependent. The droplet vaporization model must provide accurate information about the instantaneous droplet size and mass, as well as the droplet's surface temperature and composition. The latter parameters determine the physical properties important in spray breakup and coalescence models such as the droplet surface tension. The spray breakup model describes the surface area of the liquid for heat transfer and vaporization. The vaporization model also provides the fuel vapor composition (in the case of a multi-component fuel) and the heat transfer rate to the droplet to calculate the fuel vapor temperature. In the case of diesel engine spray modeling using KIVA II, the spray model calculates the simultaneous heat up and vaporization of thousands of droplets whose sizes range over several orders of magnitude. The droplet vaporization model must be numerically efficient such that the total computing time is not excessive. Detailed numerical vaporization models are available and are useful in studies of single droplet vaporization [4], but they are generally too complex for direct use in spray calculations. The main focus of this paper is to investigate the role of the vaporization model in predictions of diesel engine combustion.

In the case of diesel sprays the oxidizing atmosphere is at a high pressure and temperature that is well beyond the critical pressure and temperature of the hydrocarbon fuel. In a high pressure and temperature environment the initially cool droplets heat up throughout their lifetime and under some cases may reach their critical temperature (Sowls [5], and Faeth et al. [6]). In a high pressure environment many commonly

* Numbers in brackets designate references listed at the end of the paper.

used vaporization model assumptions are not appropriate and need modification.

MODEL FORMULATION

The numerical model is based on the KIVA-II code [3] with improvements in the vaporization and other models. The RNG (Renormalization Group) k-ε turbulence model [7], modified for the variable-density engine flows [8] is used. The spray model is a wave breakup model [9] which is further modified to account for spray wall-impingement effects, and is also improved by considering droplet distortion to obtain dynamically varying drop drag coefficients [10]. The ignition model is based on the multistep Shell ignition model [11]. The combustion model extends the laminar-and-turbulent characteristic-time model of Abraham et al. [12], which was originally developed for SI engine combustion, to simulate diesel combustion. NOx is modeled with the extended Zel'dovich mechanism [13] and soot emissions are modeled with the Hiroyasu formation model [14] and the Nagle and Strickland-Constable oxidation model [15] as described by Patterson et al. [16].

VAPORIZATION MODELS - The classic droplet vaporization model is the Spalding [17] type model as originally used in KIVA [3]. As the details of this model are well documented [3] only the main equations and important limiting assumptions will be presented here. The features of vaporization models are also summarized in Table 1. Assuming the gas phase is quasi-steady, and that the droplet surface regression rate of the droplet is small, the total energy conducted from the surrounding gas to the droplet surface (Q_d) is given as,

$$Q_d = \frac{K_{air}(T)(\hat{T}_\infty - T_d)}{2r}\ Nu_d \qquad (1)$$

where Nu_d is the Nusselt number for convective flow over a vaporizing droplet. For the case of no convective flow, and no mass transfer, Nu_d=2. For the case where there is convective flow over a sphere, Ranz and Marshall [18] give a semi-empirical Nusselt number as,

$$Nu_d = [2.0 + C_1\, Re_d^{1/2}\, Pr_d^{1/3}]$$

where C_1 is 0.6, and the Reynolds number is determined based on the free stream conditions and the Prandtl number is usually calculated from an average film condition. The convective correction is of the same form as that given previously by Frossling [19], but C_1=.55 in the Frossling correlation.

For the case of a vaporizing droplet the Nusselt number given by the Spalding model is,

$$Nu_d = [2.0 + 0.6\, Re_d^{1/2}\, Pr_d^{1/3}]\frac{ln(1+B)}{B} \qquad (2)$$

where B is the Spalding mass transfer number given by,

$$B = \frac{(W_{f,s} - W_{f,\infty})}{(1 - W_{f,s})} \qquad (2a)$$

where W_f is the mass fraction of fuel in the vapor phase. The subscript "s" refers to the droplet surface and the subscript "∞" refers to the free stream conditions. Similarly, the Spalding model gives the Sherwood number for mass transfer as

$$Sh_d = [2.0 + 0.6\, Re_d^{1/2}\, Sc_d^{1/3}]\frac{ln(1+B)}{B} \qquad (3)$$

Standard Spalding Model	**Present High Pressure Model**
Pure Fluid at Droplet Surface	Mixture at Surface Gas Diffusion into Droplet
Ideal Solution/ Ideal Gas $Y_f=P_{satf}/P$ $X_f=1.0$	Non-ideal solution Peng Robinson EOS X_f, Y_f from min. Gibbs Free Energy $x_A\hat{f}_A^l = y_A\hat{f}_A^g$ $x_B\hat{f}_B^l = y_B\hat{f}_B^g$
Ideal Laten Heat=f(T)	Enthalpy of Vaporization, $(\bar{H}_A^g - \bar{H}_A^l)$
Uniform Liq. T (Lumped)	Conduction into Droplet (2-Zone)
Constant Liq Density	Variable Liq. Density
Le=1, Bt=Bm	Le ≠ 1, Bt≠Bm
Ideal Surface Tension, f(T)	Surface Tension= f(T, P, X_f, Y_f)

Table 1: High Pressure model vs. Spalding model

Equations (1, 2, 2a) combine to give the energy conducted from the droplet surface as

$$Q_r = -2\pi r k_g (T_\infty - T_d)[2.0 + 0.6\, Re_d^{1/2}\, Pr_d^{1/3}]\left(\frac{ln(B+1)}{B}\right) \qquad (4)$$

where r is the drop radius and k_g is the gas thermal conductivity. The mass transfer from the droplet is

$$\dot{W}_A = 2\pi r \rho D_{AB}\, ln(B+1)[2.0 + 0.6\, Re_d^{1/2}\, Sc_d^{1/3}] \qquad (5)$$

where D_{AB} is the binary diffusion coefficient of fuel vapor in air. The liquid/vapor interface boundary condition of the Spalding model given above is based on Film Theory for the case of unidirectional diffusion with high mass transfer rates. This is applicable for the case where no gas is dissolved into the liquid and the

vaporization rate is large relative to the rate of diffusion. The assumption of high mass transfer rate may not be valid when the droplet is relatively cool, as in the early stages of heat-up or when vaporizing slowly.

Starting with the fundamental equation of energy transfer, and the assumptions listed above, Spalding derived the transfer number B_T for energy as

$$B_T = \frac{C_p(T_\infty - T_s)}{Q}$$

where Q is all the energy reaching the droplet per unit mass vaporized. From the assumption that Le = 1, for a vaporizing droplet the mass and energy transfer numbers must be equal. If the pressure and temperature in the bulk gas (far from the droplet) are known, and the thermophysical properties of the fuel and gas are known as a function of pressure and temperature, the surface temperature can be found. Since $W_{f,s}$ and Q are functions of the surface temperature and pressure, there is one equation and one independent variable.

An important modification to the Spalding model was proposed by Abramzon and Sirignano [20]. The modification is based on the experimental correlation of Renksizbulut and Yuen [21]. The development of the Abramzon and Sirignano model is essentially the same as the Spalding model, but now the Nusselt number for Re>25 is given by,

$$Nu_d = [2.0 + C_1 Re_d^{1/2} Pr_d^{1/3}] \frac{1}{(1+B_T)^{0.7}} \qquad (6a)$$

where B_T is the Spalding thermal transfer number, C_1=.57, and the Prandtl number and the viscosity in the Reynolds numbers are calculated at an average film condition. The Sherwood number for mass transfer is given by,

$$Sh_d = [2.0 + C_1 Re_d^{1/2} Pr_d^{1/3}] \frac{1}{(1+B_M)^{0.7}} \qquad (6b)$$

where B_M is the Spalding mass transfer number given in Eq. (2a). For conditions where the Reynolds number is low, Eqs. (6a) and (6b) are similar to the Spalding model. Renksizbulut and Yuen suggested using a 1/2 rule for the film properties, but Abramzon and Sirignano recommend a 1/3 rule (film properties are evaluated at conditions that are 1/3 the free stream conditions and 2/3 of the droplet surface conditions).

The model of Abramzon and Sirignano also incorporated a finite conduction limit in the liquid droplet to eliminate the assumption of uniform liquid temperature. The method required setting up a grid of up to 100 intervals in the radial direction inside the droplet which greatly increased the calculation time. Detailed droplet vaporization models have shown the importance of conduction within the droplet [4][20][22][23] but their added complexity and computational effort makes them inappropriate for many practical spray calculations.

All of the models described thus far are of the same general type. In all of these models the gas phase is assumed quasi-steady, i.e. the transient term $\partial(\rho w_f)/\partial t$ in the gas phase is assumed to be insignificant. However, this assumption may not be valid for high pressures where the vapor density is high. Experiments show that in a high pressure environment the ambient gas can dissolve into the liquid surface [24]. The dissolved gas effects not only the equilibrium mole fraction of the fuel in the vapor phase, but also important properties of the liquid such as its surface tension and enthalpy of vaporization. In the very high pressure atmosphere inside a diesel engine the equilibrium mole fraction of nitrogen dissolved into a tetradecane droplet may reach as high as 40%, as shown in Fig. 1. Also, in this high pressure environment ideal gas and the ideal solution assumptions may not be valid.

To account for these real gas effects the Peng-Robinson equation of state was used in the present study to calculate the partial molar fugacities of each component in both the liquid and vapor phase as well as to calculate the enthalpy of vaporization. The droplet/atmosphere interface is assumed to be in thermodynamic equilibrium unless the critical mixing point is reached. The assumption of thermodynamic equilibrium at the droplet interface may not be strictly true under conditions of very high mass transfer rates, [25] but this assumption is made here.

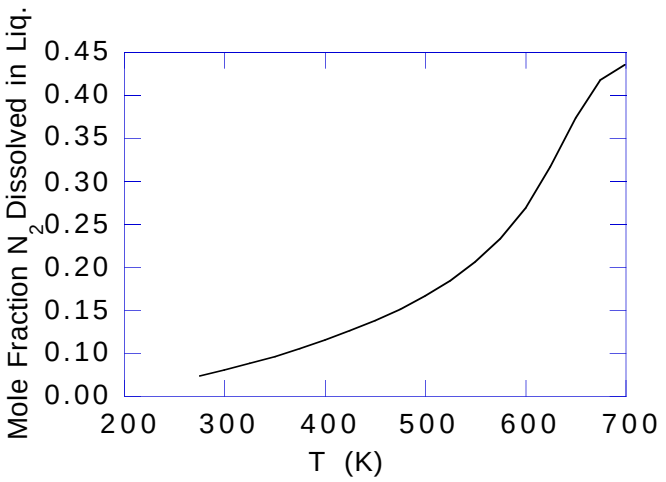

Figure 1: Calculated mole fraction of nitrogen dissolved into liquid n-tetradecane at a pressure of 91 atmospheres. Equilibrium composition calculated using the Peng-Robinson equation of state.

The condition for thermodynamic equilibrium is [26] $dG_{T,P}$=0, where $G_{T,P}$ is the Gibbs function. For a multi-component system the above equation is equivalent to

$$x_A \hat{f}_A^l = y_A \hat{f}_A^g$$
$$x_B \hat{f}_B^l = y_B \hat{f}_B^g$$

where $\hat{f}_j^i$ is the partial molar fugacity of component j in the mixture in phase i. The mole fractions of component j in the liquid and gas phases are given by x_j and y_j. The partial molar fugacity for component i in a mixture can be found from the thermodynamic relationship [27]

$$ln\frac{\hat{f}_i}{y_i P} = \int_0^v [\frac{1}{v} - \frac{1}{\bar{R}T}(\frac{dP}{dn_i})_{T,P,n_j}]dv - ln\,Z \qquad (7)$$

with a suitable equation of state to describe the pressure-volume-temperature (P-V-T) behavior of the liquid and vapor. In Eq. (7), v is the molar specific volume of the mixture, P is the pressure, T is the temperature, Z is the compressibility factor, $\bar{R}$ is the universal gas constant and n_i refers to the number of moles of component i. At low pressures the ideal gas equation adequately describes the P-V-T behavior of most gases. At high pressures, near the vapor dome, or especially near the critical point of the vapor, the ideal gas relations are no longer satisfactory [26]. A variety of equations of state exist to predict vapor-liquid-equilibrium (V-L-E) or enthalpy departure. The Peng-Robinson equation of state (EOS) is a modification of the Redlich-Kwong two-constant EOS. The Peng-Robinson EOS is given by

$$P = \frac{\bar{R}T}{v-b} - \frac{a(T)}{v(v+b)+b(v-b)} \qquad (8)$$

where a and b are

$$a = \sum_i \sum_j x_i x_j a_{ij}$$

$$b = \sum_i x_i b_i$$

where $a(T)$ is now a function of temperature as well as the critical temperature and critical pressure of the gas. The b_i and a_{ij} terms are given by

$$b_i = \frac{\Omega_{b_i} R T_{c_i}}{P_{c_i}}$$

$$a_{ii} = \frac{\Omega_{a_i} R^2 T_{c_i}^{2.5}}{P_{c_i}}$$

$$a_{ij} = \frac{(\Omega_{a_i} + \Omega_{a_j}) R^2 T_{c_{ij}}^{2.5}}{2P_{c_{ij}}}$$

where T_{c_i}, P_{c_i}, are the critical temperature, pressure, and volume of component i, respectively. The constants Ω_{a_i} and Ω_{b_i} are dimensionless constants equal to 0.4278 and 0.0867, respectively, if the first and second isothermal derivatives of pressure with respect to volume are set equal to zero at the critical point. The ij subscripts refer to parameters that are characteristics of i-j interactions and

$$P_{c_{ij}} = \frac{z_{c_{ij}} R T_{c_{ij}}}{\upsilon_{c_{ij}}}$$

$$z_{c_{ij}} = 0.291 - 0.08(\frac{\omega_i + \omega_j}{2})$$

$$T_{c_{ij}} = (T_{c_i} T_{c_j})^{1/2}(1 - k_{ij})$$

$$v_{c_{ij}} = (\frac{v_{c_i} + v_{c_j}}{2}) \text{ for gases with } \frac{v_{c_i}}{v_{c_j}} < 3 \text{ or liquids}$$

$$v_{c_{ij}}^{1/3} = (\frac{v_{c_i}^{1/3} + v_{c_j}^{1/3}}{2}) \text{ for gases with } \frac{v_{c_i}}{v_{c_j}} > 3$$

where the binary interaction coefficient, k_{ij}, is a measure of the deviation from the geometric mean for $T_{c_{ij}}$. It can be considered to be independent of temperature, density, and composition [27]. The acentric factors ω_i and ω_j, which are a measure of acentricity or the non-central nature of the intermolecular forces, are also needed to get an average acentric factor which is in turn used to evaluate an average compressibility factor ($z_{c_{ij}}$) by the Pitzer correlation for normal fluids [27]. The addition of the b(v-b) term in the denominator of the second (attractive forces) term results in greatly improved liquid density predictions [28]. The Peng-Robinson EOS has been found to give more accurate vapor-liquid equilibrium calculations than the Redlich-Kwong equation under a wide range of conditions, but especially under high pressure conditions [28].

The Peng-Robinson EOS gives the critical compressibility (Z_c) value that agrees better with experimental results than that predicted with the Redlich-Kwong and Redlich-Kwong-Soave EOS. This improvement in Z_c improves the P-V-T predictions near the critical point. For any given binary mixture the Peng-Robinson EOS utilizes an empirically derived binary interaction coefficient to account for interactions between the dissimilar molecules to increase the accuracy of the predictions. As no experimental data for the n-tetradecane/nitrogen system was available, the binary interaction coefficient used in this study was taken from the n-decane/nitrogen system from Knapp et al. [29] (k_{ij} =0.11) who compared four equations of state to experimental VLE data.

In the standard Spalding model the droplet is assumed to have a uniform temperature due to the mixing effect of internal droplet circulation. Detailed droplet vaporization models have shown that conduction into the droplet is important [4][22][23]. If conduction into the droplet is calculated, the droplet surface temperature rises faster than the temperature of the rest of the droplet. A faster surface temperature response increases both the initial vaporization rate and the rate of droplet breakup by decreasing the liquid surface tension. In spray combustion models the details of the temperature and composition within the droplet are not required, only an accurate representation of the droplet surface and the bulk droplet properties.

In the present study a simplified method of calculating conduction into the droplet, without the complexity of introducing a numerical grid within the droplet, was introduced, called a 2-zone model. The 2-zone model uses a thin outer boundary layer to represent the droplet surface properties and an inner zone to represent the rest of the droplet, as depicted in Fig. 2. The outer boundary layer thickness was assumed to be proportional to the square root of the effective thermal diffusion rate times the droplet lifetime. If a droplet breaks up or coalesces with another droplet it is assumed that the event causes instantaneous mixing within the droplet and a new outer boundary is formed. Also, the new droplets have the average properties of the parent(s). As the initial droplet thermal boundary layer would have zero thickness, it is assumed that the initial boundary layer contains 10 % of the total droplet volume. This was found to be advantageous for numerical stability.

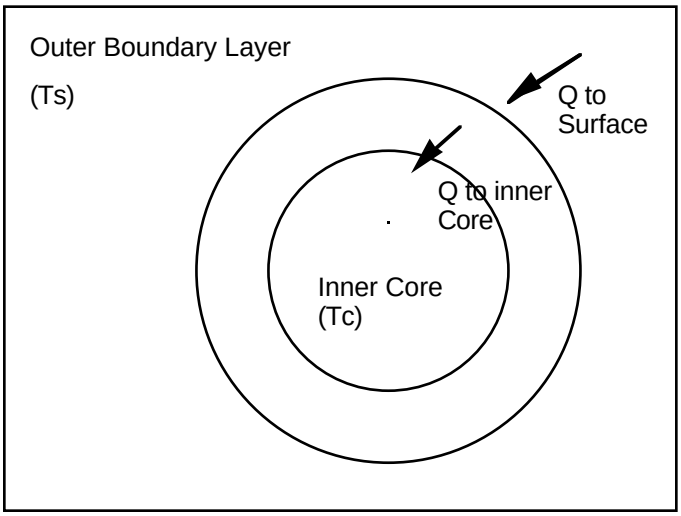

Figure 2: Schematic diagram of the 2-zone droplet vaporization model.

Another advantage of using the present 2-zone droplet vaporization model under high pressure conditions is that, with a uniform temperature, the whole droplet reaches its critical temperature at the same time. Since it is not clear what happens to a droplet that has reached its critical temperature, often it is assumed the whole droplet has "vaporized" [3]. With the current 2-zone model, if the outer boundary layer reaches its critical temperature, only the outer layer is assumed to be vaporized.

Conduction from the droplet surface to the center of the droplet is enhanced by the flow circulation within the droplet [30]. Jin and Borman [30] estimated an effective liquid conductivity and mass diffusivity to account for circulation in the droplet interior. The effective liquid transport properties were found to range from 2.685 to 4.208 times the quiescent values by using the following equation [30].

$$C = 2.685 + \frac{3.02514x10^{-3}}{1.9868x10^{-3} + D_{12}\frac{t}{r^2}}$$

$$\text{for } 0.0004 \le D_{12}\,{}^{t}\!/_{r^2} < 1$$

$$C = 2.685 \qquad \text{for } D_{12}\,{}^{t}\!/_{r^2} \ge 1$$

For this study a representative thermal transport correction factor of 3.0 was used to account for the enhanced thermal diffusion rate within the droplet.

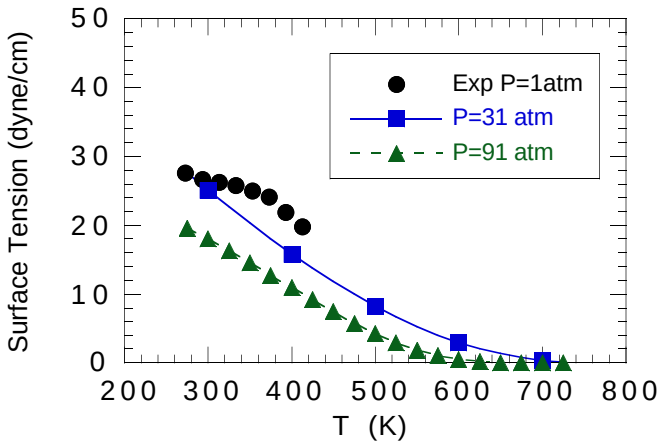

Figure 3: The effect of pressure on the surface tension of n-tetradecane in a nitrogen environment using the Maclead-Sugden correlation.

Because of the high pressure environment in a diesel engine, thermodynamic and transport properties also need to account for the effects of pressure. In the standard Spalding model the Lewis number is assumed equal to 1. In a high pressure environment the Lewis number may vary from 1 to 4 [22]. In the present high pressure model the mass transfer number and thermal transfer number are not assumed to be equal, but are calculated separately. The enthalpy of vaporization is equal to the difference between the partial molar enthalpy of species A in the saturated vapor and the partial molar enthalpy of species A in the saturated liquid. In low pressure calculations, this difference is often approximated by the latent heat of vaporization, L, of the pure fluid into its own pure vapor. Manrique and Borman

showed that at high pressures this simplifying assumption could lead to large errors [31]. Manrique and Borman used the enthalpy departure function in the vapor phase to correct the ideal latent heat for the high pressure droplet vaporization case. The technique of Manrique and Borman applied to both the liquid and vapor phases using the Peng-Robinson equation of state was also used in this study.

In spray breakup models a primary physical property is the droplet surface tension. In most low pressure models, and in the original KIVA code [3], the surface tension of the pure fuel is used. At high pressures the ambient gases dissolved into the liquid have an important effect on the surface tension. For this study the surface tension of the liquid mixture was calculated using the Maclead-Sugden correlation [27] given by,

$$\sigma_m^{1/4} = \sum_i p_i [x_i \rho_{m,l} - y_i \rho_{m,g}]$$

where p_i is the parachor of component i, x_i is the mole fraction of component i in the liquid phase, y_i is the mole fraction of component i in the vapor phase, $\rho_{i,j}$ is the density of component i in phase j. A sample calculation of the surface tension of n-tetradecane in a high pressure nitrogen atmosphere is shown in Fig. 3. The experimental low pressure surface tension of pure n-tetradecane is given for comparison. The amount of nitrogen dissolved into the n-tetradecane increases with increasing ambient pressure and increasing liquid temperature. The dissolved nitrogen at high pressures is seen to greatly reduce the surface tension of the liquid [32].

A summary of common assumptions used in the Spalding model and the models used in the present study are shown in Table 1.

RESULTS AND DISCUSSION

The KIVA-II code was modified by replacing the standard Spalding model (see Table 1) with the High Pressure model. Before applying the model to diesel sprays, single droplet computations were done to examine the behavior of the High Pressure model, then the KIVA-II code with both models was run separately to simulate the vaporizing spray experiments of Kamimoto et al. [33] and Hou at al. [34] before simulating the combustion process in the Caterpillar engine.

SINGLE DROPLET - To assess the influence of drop vaporization models the models were first applied to a single tetradecane drop in a stagnant nitrogen environment at 80 atm pressure and 900 K temperature. The drop initial radius, R_0, was 10 μm.

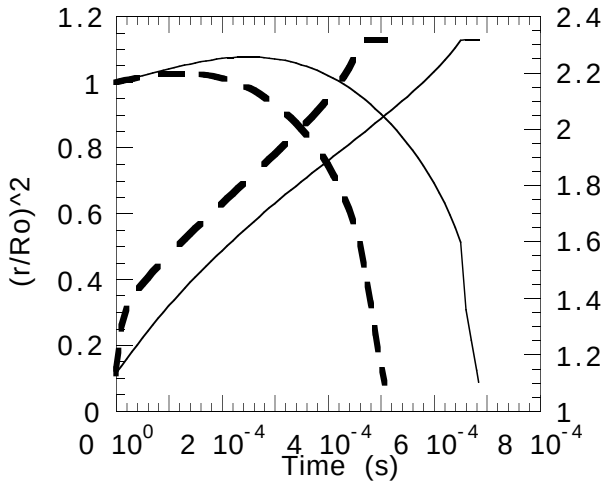

Figure 4: Comparison of droplet surface temperature and size during vaporization by using the standard Spalding model (with variable liquid density included) (solid line) and the present High Pressure model (dashed line).

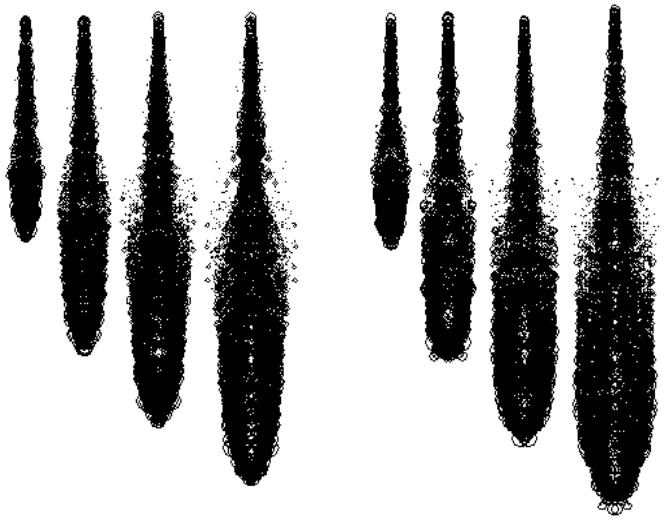

Figure 5: Spray prediction of the Kamimoto experiment by High Pressure and Spalding models at 0.5, 1.0, 1.5, and 2.0 ms.

Unlike the Spalding model which assumes uniform temperature for a fuel droplet, the High Pressure model represents the droplet surface temperature more accurately by using the 2-zone approximation explained in the previous section. A faster surface temperature response is achieved due to better simulation of the fuel droplet surface temperature, which increases the rate of vaporization as seen in Fig. 4, even when variable liquid density is considered in the Spalding model.

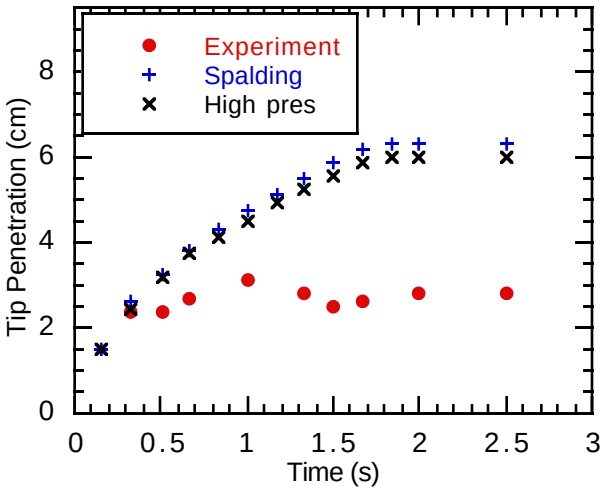

(a)

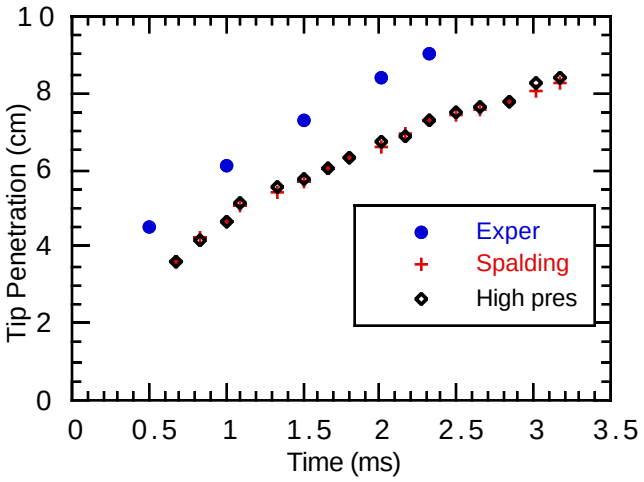

(b)

Figure 6: The predictions of (a) the spray and (b) the fuel vapor tip penetration of the Kamimoto et al. [33] experiment.

SPRAY VAPORIZATION - The effect of the High Pressure and Spalding models on spray vaporization was tested by comparing the models to the experiments done by Kamimoto et al. [33] and Hou et al. [34]. The computations were done in 2 dimensions with 0.7x0.7 mm cell sizes. The results were found to be adequately grid size independent with this selection of mesh size.

Kamimoto - To simulate spray vaporization, tedradecane fuel was injected into a quiescent nitrogen-filled bomb at a pressure of approximately 3.1 MPa and a temperature of 900 K using the experimental condition of the Kamimoto experiments. The nozzle diameter, the nozzle L/D ratio, and the injection pressure were 0.016 cm, 3.125, and 110 MPa respectively. The results are shown in Fig. 5 which shows the sprays at various time steps. The spray drop locations are indicated by the circles. The size of the circles represents the mass of liquid contained in each drop parcel. Figure 6 shows the spray and vapor tip penetrations as a function of time. Both models over-predict the spray penetrations and under-predict the vapor penetrations. The prediction of

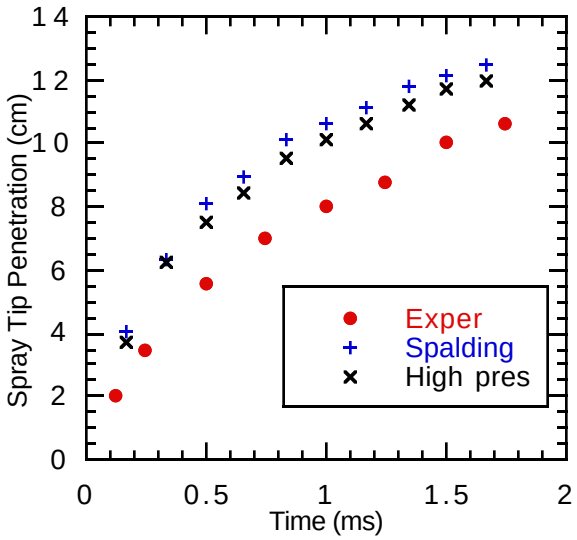

(a)

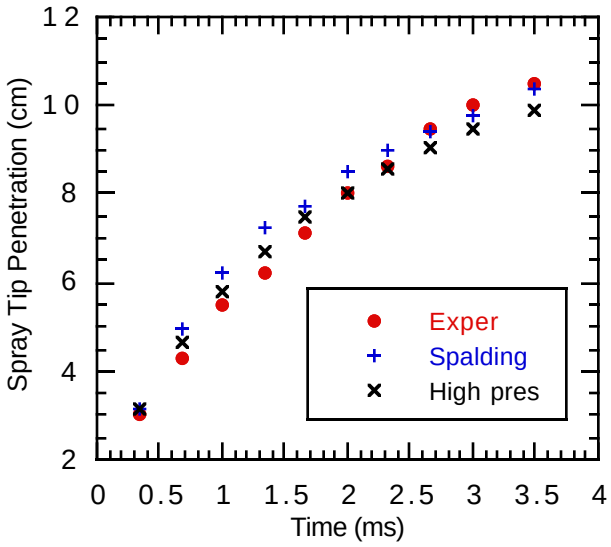

(b)

Figure 7 Prediction of the vaporizing liquid spray penetration of the Hou et al. [34] experiment at (a) 4.2 MPa (P_{inj}=138 MPa) and (b) 13.1 MPa (P_{inj}=142 MPa) ambient pressures.

Cylinder bore x stroke (mm)	137.6 x 165.1
Connecting rod length (mm)	261.62
Displacement volume (L)	2.44
Compression ratio	15.1
Number of nozzle orifice x diameter (mm)	6 x 0.259
Spray angle (from cylinder head)	27.5 degrees
Combustion chamber	Quiescent
Piston crown	Mexican hat
Inlet air pressure	184 kPa
Inlet air temperature	310 K
Intake valve closure	–147 deg. ATDC
Swirl ratio (nominal)	1.0
Engine speed	1600 rpm
Fuel	Amoco Premier #2
Injection system	Common Rail
Injection pressure	90 MPa
Fuel injected	0.1622 g/cycle
Overall equivalence ratio	0.46
Injection duration	21.5 crank angle degrees
Start of injection	–15, –11 (baseline case) and –5 deg. ATDC

Table 2: Caterpillar Engine Conditions

the high pressure model shows a very slight improvement of the spray penetration.

Hou - Diesel # 2 fuel was injected into a quiescent nitrogen-filled bomb at a pressure of 4.2 MPa and 13.1 MPa and a temperature of 900 K. The nozzle diameter and the injection pressures were 0.032 cm and 138 MPa and 142 MPa. The spray tip penetration predictions, shown in Fig. 7, again show that only a slight improvement is achieved by using the High Pressure vaporization model. However the differences between the models is small. A possible explanation for this is that very small drops are predicted to be the outcome of the atomization process by the present spray model. These small drops rapidly reach their critical temperature and disappear. The larger parent drops vaporize more slowly and, under these relatively low drop temperature conditions, the two models predict similar drop vaporization rates.

Overall predictions of the spray tip penetration for Kamimoto and Hou experiments indicate that the predictions agree with the experimental results at the very early time steps and over predict the spray penetrations at later time steps. Further work needs to be done to improve the spray model.

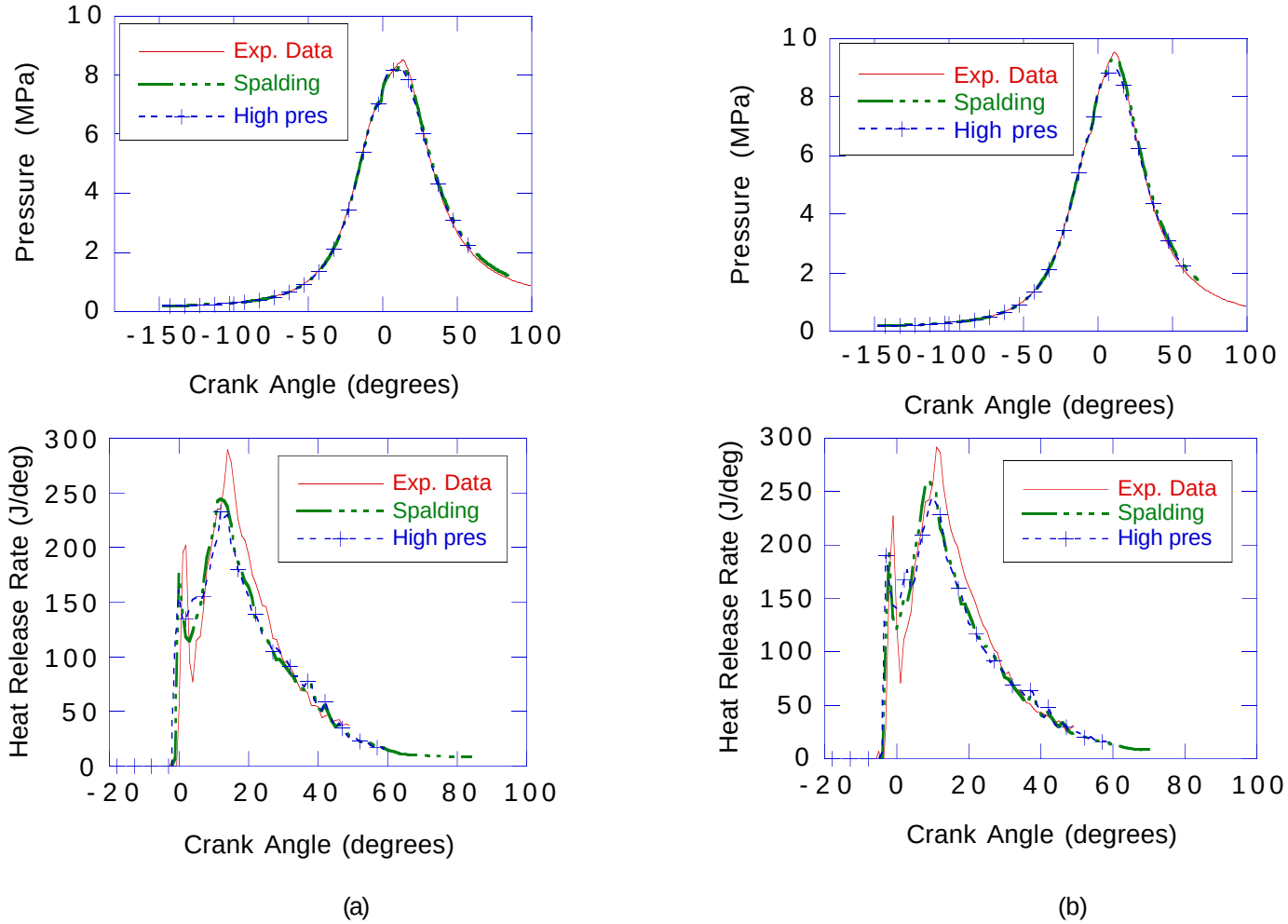

Figure 8: Cylinder pressure (top) and heat release rate (bottom) predictions. Injection timing (a) -8 degrees ATDC, (b) -11 degrees ATDC.

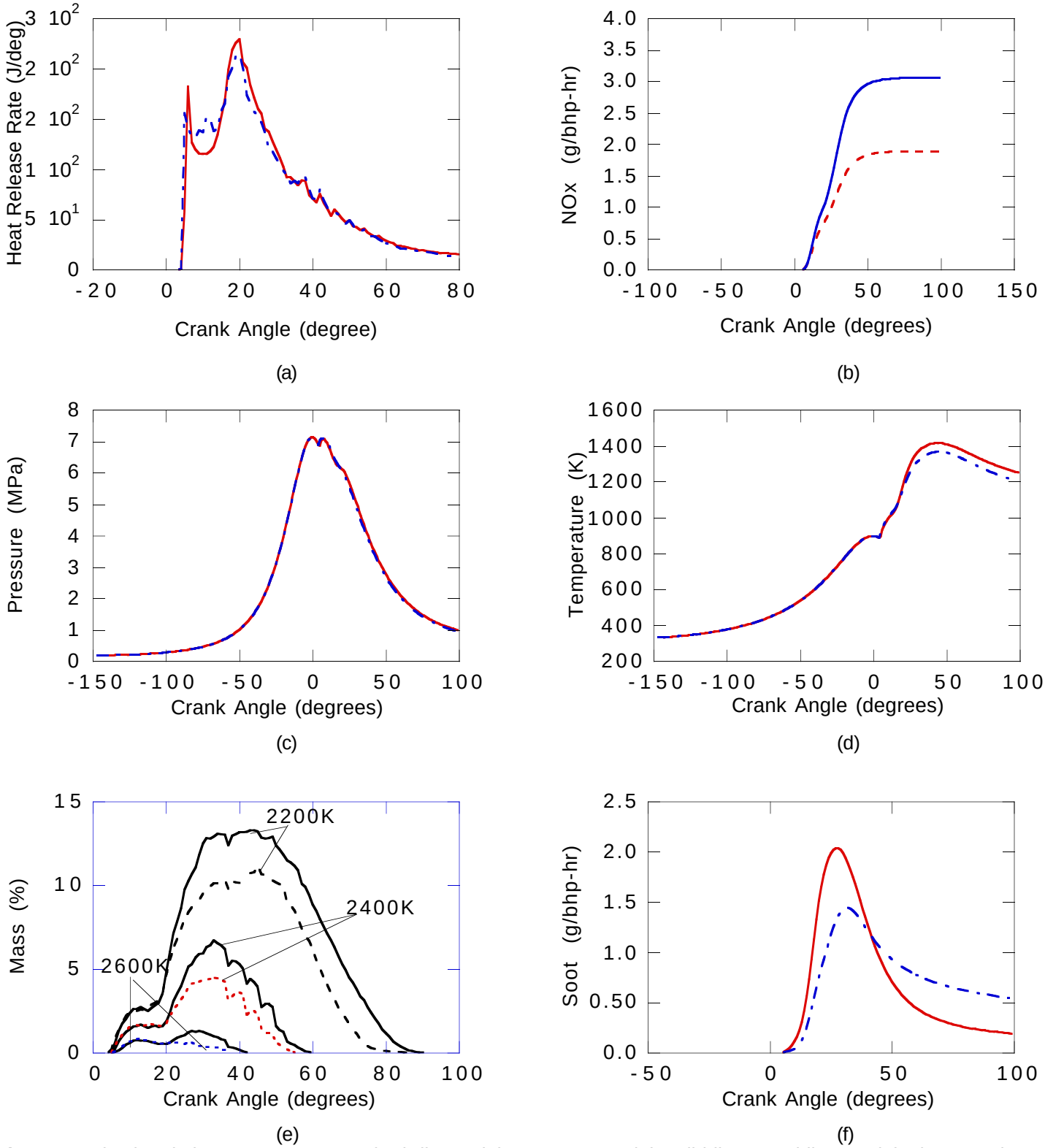

Figure 9: Injection timing -2.5 ATDC. Dashed lines-High Pressure model, solid lines-Spalding model. a) Heat release rate, b) total cylinder NOx evolution, c) cylinder pressure, d) average cylinder temperature, e) percent of cylinder mass with temperatures above the indicated values, f) total cylinder soot evolution.

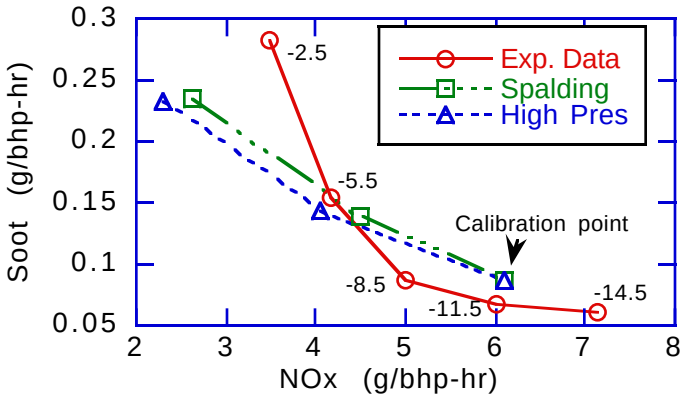

Figure 10: Measured and computed emission data for different injection timing, -2.5, -7.5, -11.0 degrees ATDC.

DIESEL COMBUSTION - The effect of vaporization models on diesel combustion predictions was studied by applying the models to simulate the overall combustion processes of a Caterpillar diesel engine. The specifications and operating conditions of this engine are listed in Table 2 [35]. The fuel delivery schedule and mass flow rate are given by Nehmer [35]. The computations used tetradecane ($C_{14}H_{30}$) as the fuel due to its similar C/H ratio to diesel fuel.

The computational mesh used represents one sixth of the combustion chamber in the engine (i.e., a 60 degree sector) for computational efficiency, since the injector has six injector holes. Thus, the computational domain had periodic boundary conditions. There were 20 cells in the radial direction, 30 cells in the azimuthal direction and 18 cells in the axial direction with 5 cells in the squish region at top dead center. This mesh resolution has been found to give adequately grid-independent results by Han and Reitz [8].

The prediction of the pressure and heat release rate by both models for different fuel injection timings are compared with the experimental data in Fig. 8. The High Pressure model predicts a higher heat release rate after the pre-mixed burn. While the pressure rises quickly after the premixed burn, the reduced heat release throughout the cycle leads to a slightly lower peak pressure. Some small improvement in the heat release rate prediction during the later part of the piston expansion stroke can be observed in Fig. 8.

Overall, the High Pressure and Spalding vaporization models produce very similar global results. One reason for this is that, in the diesel environment, like in the Kamimoto experiments, the small droplets produced during the atomization process quickly reach their critical temperatures and enter the vapor phase. This makes the details of the vaporization process less important than in other drop vaporization regimes. The High Pressure model does produce somewhat lower in-cylinder temperatures, as seen in Fig. 9 for a retarded timing case. Since the NO formation is extremely sensitive to the in-cylinder temperature, significantly less NOx emission is predicted, as seen in the same Figure. Also, while lower in-cylinder temperatures decrease the formation of soot, the final amount of soot shows a net increase caused by the correspondingly lower oxidation rate. These trends were also seen at the other injection timings considered in the study.

To facilitate comparisons with the measured data, the models were 'calibrated' at one operating point. The NOx emissions results for the Spalding model were multiplied by the calibration factor, $\beta = 0.78$. The high pressure model used $\beta = 1.10$. The procedure used to adjust the soot model was to ensure that the baseline case (the -11 degree case) emissions agreed reasonably with the experimental data by adjusting A_f in the Hiroyasu formation rate expression, with A_f=320 for the Spalding model and A_f=118 for the High Pressure model. The predictions show that the High Pressure models produce a similar Soot-NOx tradeoff curve as for the Spalding model results, as seen in Fig. 10. However, both models underestimate the soot levels at very retarded timings. Some reasons for this are discussed by Hampson and Reitz [36].

Although the two different vaporization models give very similar heat release and emissions results, there are differences later in the expansion stroke. The standard Spalding model, as seen in Fig. 11a predicts significant liquid fuel remaining in the combustion chamber at the end of the combustion process. The present High Pressure model, on the other hand, shows a great improvement since much smaller unevaporated liquid fuel concentrations are seen in Figs. 11 and 12. This improvement in the predictions is due to more realistic accounting for high pressure real gas effects in diesel combustion.

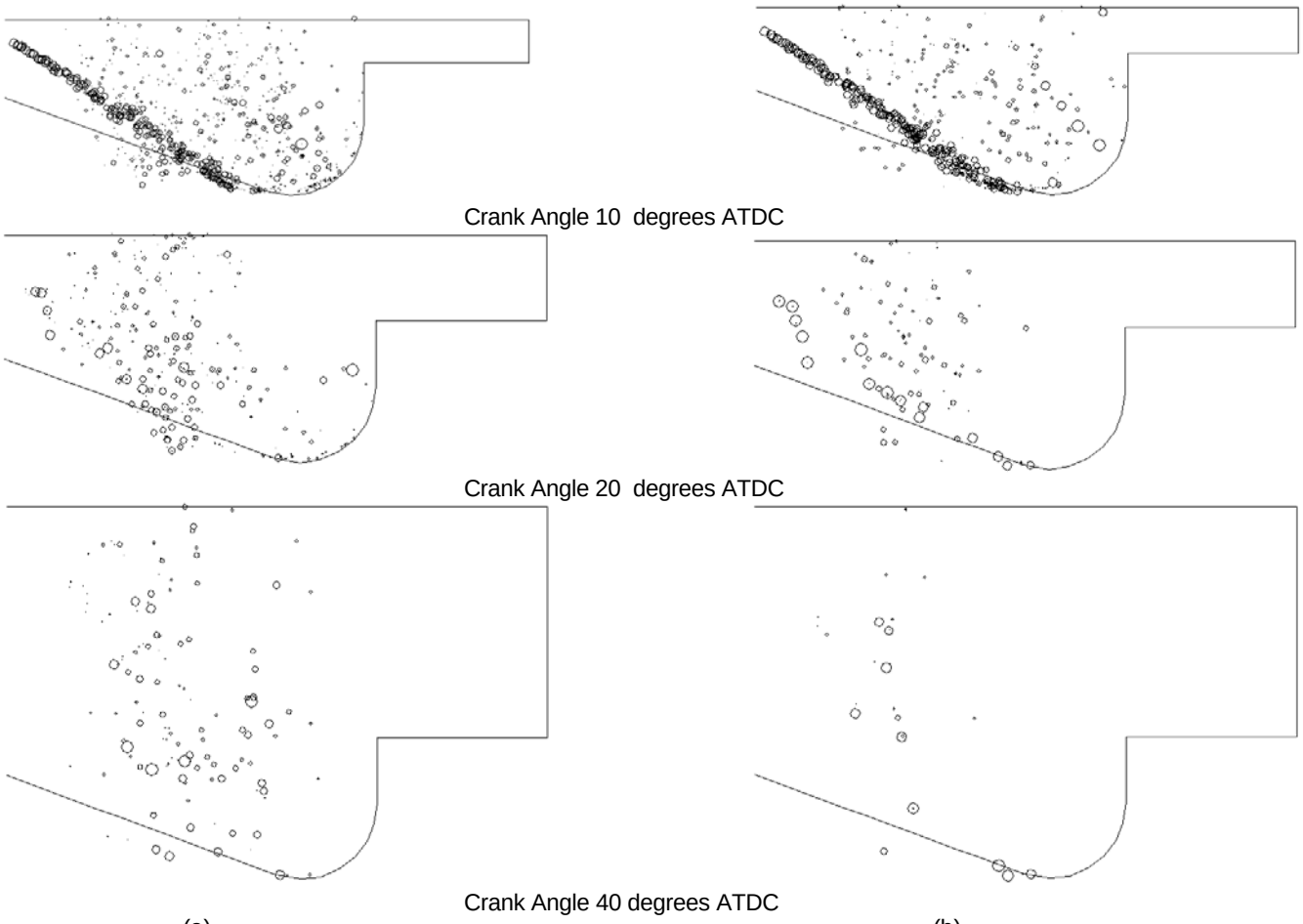

Figure 11: Liquid fuel parcel location predictions at 10, 20, and, 40 crank angle ATDC. Injection timing is -11 ATDC. (a) Spalding model, (b)present High Pressure model.

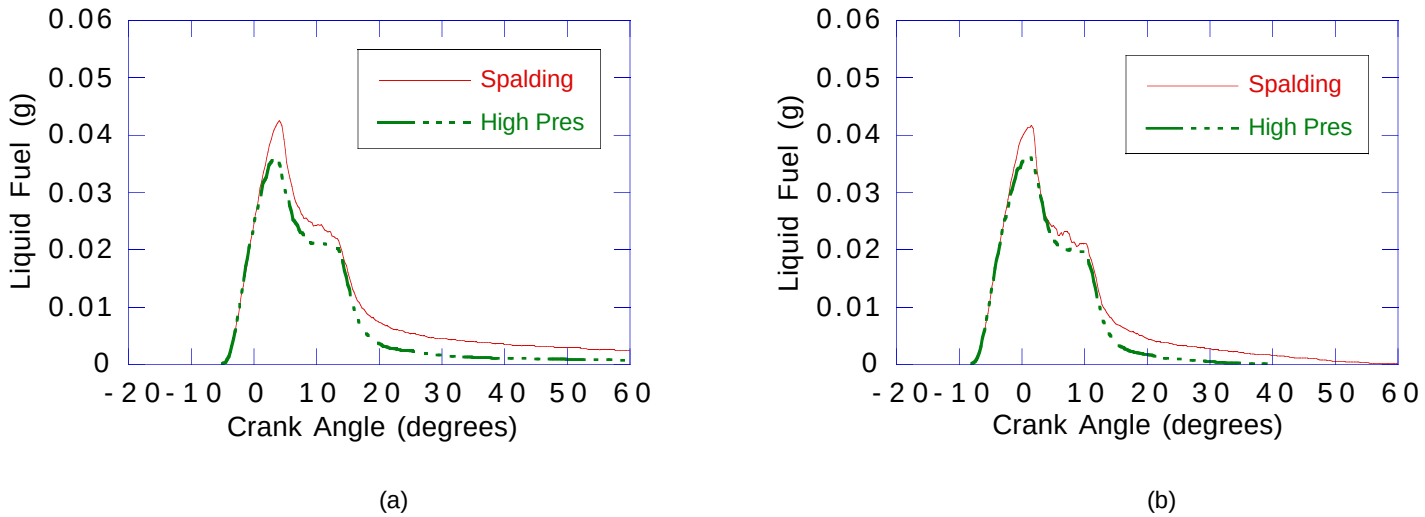

Figure 12: Total unevaporated liquid fuel in the combustion chamber. Injection timing (a) -8 degrees ATDC, (b) -11 degrees ATDC.

SUMMARY AND CONCLUSIONS

The KIVA code has been used to explore the performance of the standard Spalding and a High Pressure vaporization model developed in this study. The improved vaporization model gives better approximations of the fuel droplet surface temperature, surface tension, fuel density, gas diffusion into the droplet, and non-ideal gas state equations. The models were first tested for single droplets and sprays, and results were compared with experiments. Then the models were tested by simulating diesel combustion in a heavy duty diesel engine.

The new high pressure vaporization model shows only a slight improvement in predicting spray penetration and the vaporization rate of the liquid fuel droplets. The

two vaporization models also give very similar heat release and emissions results in the engine computations. The reason for the similar performance is related to the fact that the spray model predicts that very small drops are produced in the atomization process and these small drops quickly reach the critical state so that the details of the vaporization model are not influential. The improved High Pressure model predicts lower in-cylinder temperatures due to earlier vaporization and therefore lower NOx emissions and higher soot; but, the NOx-versus-soot tradeoff prediction does not change significantly. However the more realistic vaporization rate predicted by the High Pressure model does improve the prediction of unburned liquid fuel remaining at the end of the combustion process significantly.

ACKNOWLEDGMENTS

The work was supported under DOE/NASA-Lewis grant NAG 3-1087 and by Caterpillar, Inc. Additional facilities and support were provided by the Army Research Office. Support for the super computations was provided by San Diego Supercomputer Center, Tacom and Cray Research, Inc.

REFERENCES

1. Obert, E. F., *Internal Combustion Engines and Air Pollution,* Harper Collins,1973.

2. Lefebvre, Arthur, H., "Gas Turbine Combustion", Hemisphere Publishing Co., 1983.

3. Amsden, A. A. , O'Rourke, P. J., and Butler, T. D.,"KIVA II: A Computer Program for Chemically Reactive Flows with Sprays", Los Alamos National Laboratory, LA-11560-MS, May, 1989.

4. Curtis, E. W. and P. V. Farrell, Combustion and Flame, Vol. 90, pp. 85-102, 1992.

5. Sowls, Richard E., *An Experimental Study of Carbon Dioxide Droplets Falling Through an Inert High Pressure High Temperature Environment.* Ph.D. Thesis, Dept. of Mech. Eng., University of Wisconsin, Madison, 1972.

6. Faeth, G. M., Dominicis, D. P., Tulpinsky, J. F., and Olson, D. R., Twelfth Symposium (International) on Combustion, The Combustion Institute, Pittsburgh, Penn., 1969.

7. Yakhot, V., and Orszag, S. A. “Renormalization Group Analysis of Turbulence. I. Basic Theory.” *J. Sci. Comput*., **1**, 3, 1986.

8. Han, Z. and Reitz, R. D. “Turbulence Modeling of Internal Combustion Engines Using RNG k-e models”, accepted for publication *Comb. Sci. Tech.*, 1995.

9. Reitz, R. D. "Modeling Atomization Processes in High Pressure Vaporizing Sprays," *Atomization and Spray Technology*, **3**, 309-337, 1987.

10. Kong, S., Han, Z., and Reitz, R. D. “The Development and Application of a Diesel Ignition and Combustion Model for Multidimensional Engine Simulation", SAE Paper 950278, 1995.

11. Halstead, M., Kirsh, L. and Quinn, C. "The Autoignition of Hydrocarbon Fuels at High Temperatures and Pressures - Fitting of a Mathematical Model," *Combust. Flame*, **30**, 45-60, 1977.

12. Abraham, J., Bracco, F. V. and Reitz, R. D. "Comparisons of Computed and Measured Premixed Charge Engine Combustion," *Combust. Flame*, **60**, pp. 309-322, 1985.

13. Heywood, J.B. 1976 "Pollutant Formation and Control in Spark-Ignition Engines*," Progress in Energy and Combustion Science*, Vol. 1, pp. 135-164, 1976.

14. Hiroyasu, H. and Nishida, K. "Simplified Three-Dimensional Modeling of Mixture Formation and Combustion in a D.I. Diesel Engine," SAE Paper 890269, 1989.

15. Nagle, J. Strickland-Constable, R. F., "Oxidation of Carbon between 1000-2000 C," Proc. of the Fifth Carbon Conf., Volume 1, Pergammon Press, p. 154, 1962.

16. Patterson, M. A., Kong, S. -C., Hampson, G. J. and Reitz, R. D. "Modeling the Effects of Fuel Injection Characteristics on Diesel Engine Soot and NOx Emissions," SAE Paper 940523, 1994.

17. Spalding, D. B., "The Combustion of Liquid Fuels", *Fourth Symposium (International) on Combustion*, The Combustion Institute, Pittsburgh, Penn., 1953.

18. Ranz, W. E., and Marshall, W. R. JR., Chem. Engr. Prog. Vol. 48, pp 141-146, 173-180, (1952).

19. Frossling, Beitr. Geophys. 52. 170-216 (1938).

20. Abramzon, B., and Sirignano, W. A., 1987 ASME/JSME Thermal Engineering Conference - Volume One, Book No. I0219A, ASME New York, 1987.

21. Renksizbulut M., and Yuen, M. C., Journal of Heat Transfer, Vol. 105, pp 384-388, May 1983.

22. Abramzon, B., and Sirignano, W. A., Int. J. Heat Mass Transfer. Vol. 32, No. 9, pp. 1605-1618, 1989.

23. Law, C. K., and Sirignano, W. A., Combustion and Flame 28, 175-186 (1977).

24. Azarnoosh, A. and J. J. McKetta, Journal of Chemical Engineering Data, Vol. 8, No. 4, October 1963, pp. 494-498.

25. Rosner, Daniel E., and Chang, W. S., *Combustion Science and Technology*, 1973, Vol. 7, pp.145-158.

26. Van Wylen, G. and Sonntag, R., *Fundamentals of Classical Thermodynamics 3rd ed.*, Wiley, 1986.

27. Reid, Robert C., Prausnitz, John M., and Poling, Bruce E., The Properties of Gases & Liquids, 4th Edition, McGraw-Hill, New York, 1987.

28. Peng, Ding-Yu and Robinson, Donald B., Ind. Eng. Chem., Fundam., Vol. 15, No. 1, 1976.

29. Knapp, H. Doring, R., Oellrich, L., Plocker, U., and Prausnitz, J.M.,Vapor-Liquid Equilibria for Mixtures of Low Boiling Substances, Chemistry Data Series, Vol. VI, DECHEMA, 1982.

30. Jin, J. D., and Borman, G. L., SAE Paper 850264, 1985.

31. Manrique, J. A. and Borman, G. L., Int. J. Heat Mass Transfer 12, 1081-1095, 1969.

32. Reno, Gordan J., and Donald L. Katz, Industrial and Engineering Chemistry, Vol. 35, No. 10, pp. 1091-1093.

33. Kamimoto, Takeyuki, H. Yokota, and H. Kobayashi, SAE Paper , 871610, 1987.

34. Hou, Z. X., Abraham, J., and Siebers, D. L., “Three Dimensional Computations of Diesel Sprays in a Very High Pressure Chamber” SAE Paper 941896, 1994.

35. Nehmer, D. A. and Reitz, R. D., "Measurement of the Effect of Injection Rate and Split Injections on Diesel Engine Soot and NOx Emissions," SAE Paper 940668, 1994.

36. Hampson G.J., and Reitz, R.D., “Development of NOx and Soot Models for Multidimensional Diesel Combustion”, ASME paper, (Submitted to the 1995 ASME International Joint Power Generation Conference, Oct. 8-12, 1995, Minneapolis, MN).